

See discussions, stats, and author profiles for this publication at: <https://www.researchgate.net/publication/340651387>

Simulation and optimization of $\text{CH}_3\text{NH}_3\text{SnI}_3$ based inverted perovskite solar cell with NiO as Hole transport material

Article in *Materials Today: Proceedings* · April 2020

DOI: 10.1016/j.matpr.2020.03.488

CITATION

1

READS

70

3 authors, including:



Shamna M S

Christ College, Irinjalakuda

1 PUBLICATION 1 CITATION

SEE PROFILE



Sudheer Sebastian

Christ College, Irinjalakuda

13 PUBLICATIONS 325 CITATIONS

SEE PROFILE



Simulation and optimization of $\text{CH}_3\text{NH}_3\text{SnI}_3$ based inverted perovskite solar cell with NiO as Hole transport material

M.S. Shamna*, K.S. Nithya, K.S. Sudheer

Christ College (Autonomous), Irinjalakuda, Thrissur 680125, University of Calicut, Kerala, India

ARTICLE INFO

Article history:

Received 9 November 2019

Accepted 17 March 2020

Available online 15 April 2020

Keywords:

Inverted perovskite solar cell

Device simulation

Electron transport material

Hole transport material

Transparent conducting oxide

Defect density

ABSTRACT

A planar perovskite solar cell (PSC) with p-i-n inverted structure is modeled and simulated using SCAPS software to determine the power output characteristics under illumination. The inverted structure is NiO/ $\text{CH}_3\text{NH}_3\text{SnI}_3$ /PCBM where NiO is the hole transport layer (HTL), $\text{CH}_3\text{NH}_3\text{SnI}_3$ is the perovskite absorber layer and PCBM is the electron transport layer (ETL). Simulation efforts are focused on thickness of three layers, defect density of interfaces, density of states, and metal work function effect on power conversion efficiency (PCE) of solar cell. For optimum parameters of all three layers, efficiency of 22.95% has been achieved. From the simulations, an alternate lead free inverted perovskite solar cell is introduced.

© 2019 Elsevier Ltd. All rights reserved.

Selection and peer-review under responsibility of the scientific committee of the International Conference on Photochemistry and Sustainable Energy (ICPSE 2019).

1. Introduction

In recent years, in the field of optoelectronic devices organometal halide perovskite solar cells (PSCs) have drawn much attention of research community due to simpler processing techniques and low manufacturing cost compared to traditional silicon based solar cells and high PCE [1]. Since first introduced $\text{CH}_3\text{NH}_3\text{PbX}_3$ PSCs have shown an exceptional efficiency growth, 3.8% in 2009 to 25.2% in 2019 [2]. Even though lead based PSC has high efficiency, as they contain lead they are toxic and can bring health and ecological hazards [3].

By using $\text{CH}_3\text{NH}_3\text{SnI}_3$ as the absorber layer, which has a direct band gap of 1.30 eV, the toxicity of typical perovskite solar cells can be avoided. It has most appreciable optical properties among all the $\text{CH}_3\text{NH}_3\text{BX}_3$ (B = Sn, Pb; X = Cl, Br, I) compounds for optoelectrical applications [4].

In PSCs, especially regular planar heterojunction PSCs, the hysteresis phenomenon is often observed one of the major issues currently holding back the further progress of it [5]. Ion migration behaviour in the perovskite film is considered to be the major origin of hysteresis [6,7]. It is observed that the inverted p-i-n device with planar structure has greatly suppresses hysteresis effects with device efficiency close to 20% [8].

The implementation of [6,6]-phenyl-C61-butyric acid methyl ester (PCBM) as electron transport material (ETM) is viewed as the key to suppress the trap states and tie up the mobile ions to form a radical [9,10]. Thus ion migration could be limited. The p-type inorganic materials like NiO are grabbing more attention due to their better stability. So NiO is an efficient hole transport material (HTM) in photovoltaic field [11].

SCAPS-1D (Solar Cell Capacitance Simulator) is a one dimensional solar cell simulation programme developed at ELIS, University of Gent. SCAPS is used for the simulation of $\text{CH}_3\text{NH}_3\text{SnI}_3$ based PSC with NiO as HTM and PCBM as ETM and the detailed analysis of the device by varying various parameters have been carried out.

2. Device structure and simulation

We have considered inverted planar heterojunction as absorber layer and PCBM as ETM along with NiO as HTM. To analyze the effect of different electrical parameters on the efficiency of Glass/ITO/NiO/ $\text{CH}_3\text{NH}_3\text{SnI}_3$ /PCBM/Al based inverted PSC structure. Fig. 1 shows the schematic device structure for the simulation and Fig. 2 shows the energy level diagram of the device.

The one-dimensional solar cell simulation program, SCAPS-1D is based on three coupled differential equations, namely, Poisson's (1), continuity equation for holes (2) and electrons (3) as follows:

$$\frac{d}{dx} \left(-\varepsilon(x) \frac{d\Psi}{dx} \right) = q [p(x) - n(x) + N_d^+(x) - N_a^-(x) + p_t(x) - n_t(x)] \quad (1)$$

* Corresponding author.

E-mail address: shamnams@christcollegeijk.edu.in (M.S. Shamna).

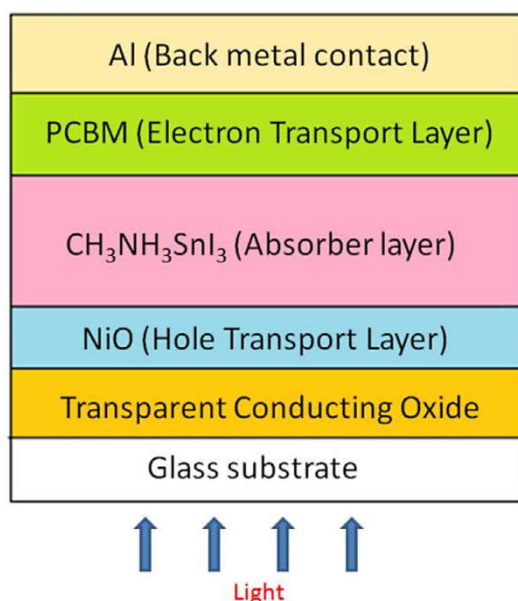


Fig. 1. Device structure for inverted PSC.

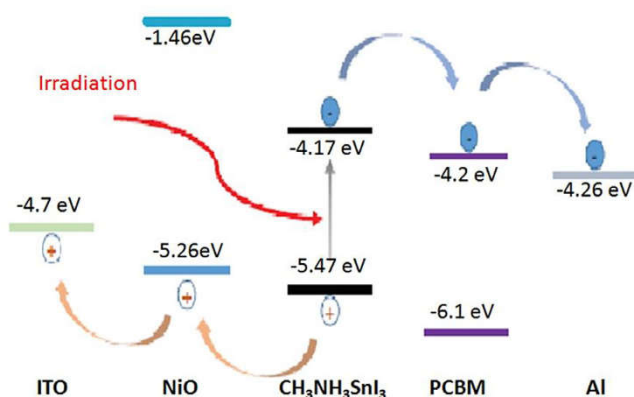


Fig. 2. Energy band diagram.

$$\frac{dp_n}{dt} = G_p - \frac{p_n - p_{n0}}{\tau_p} - p_n \mu_p \frac{d\zeta}{dx} - \mu_p \zeta \frac{dp_n}{dx} + D_p \frac{d^2 p_n}{dx^2} \quad (2)$$

$$\frac{dn_p}{dt} = G_n - \frac{n_p - n_{p0}}{\tau_n} + n_p \mu_n \frac{d\zeta}{dx} + \mu_n \zeta \frac{dn_p}{dx} + D_n \frac{d^2 n_p}{dx^2} \quad (3)$$

Here ϵ is dielectric constant, Ψ is the electrostatic potential, q is electron charge, D is diffusion coefficient, ζ is permittivity and n , p , n_t and p_t are free electrons, free holes, trapped electrons and trapped holes respectively. N_a^- refers to ionized acceptor-like doping concentration and N_d^+ for ionized donor like doping concentration. The simulation is done under an illumination of 1000 W/m^2 , temperature of 25°C and an air mass of 1.5 G [12].

The values of device and material parameters are adopted from theories and literatures [13–15] for simulation are summarized in Table 1–3. Using optimum values of different electrical parameters for inverted PSC, the finally obtained simulated device performance parameters such as short-circuit current density J_{sc} , open-circuit voltage V_{oc} , fill factor FF and PCE is shown in Table 4.

3. Results and discussion

3.1. Effect of thickness of the $\text{CH}_3\text{NH}_3\text{SnI}_3$, ETM and HTM layers

Thickness of the absorber layer has great influence on the overall performance of the solar cell. Thickness of $\text{CH}_3\text{NH}_3\text{SnI}_3$ has been varied from 300 nm to 1100 nm with NiO as HTM layer and PCBM

Table 2
Parameters of interface layer.

Interface layer	ETL/Perovskite layer	Perovskite layer/HTL
Defect type	Neutral	Neutral
Capture cross section electrons (cm^2)	1×10^{-19}	1×10^{-19}
Capture cross section holes (cm^2)	1×10^{-19}	1×10^{-19}
Energetic distribution	Single	Single
Reference for defect energy level E_t	Above the highest E_v	Above the highest E_v
Energy with respect to reference (eV)	0.600	0.600
Total density (integrated over all energies) ($1/\text{cm}^3$)	1×10^{10}	1×10^{10}

Table 1
Parameters used for simulation of inverted perovskite solar cell using SCAPS-1D.

Parameters	PCBM (ETL)	$\text{CH}_3\text{NH}_3\text{SnI}_3$	NiO (HTL)
Thickness (nm)	85	600	30
Bandgap (eV)	2.0	1.3	3.8
Electron affinity (eV)	4.2	4.17	1.46
Dielectric permittivity (relative)	3.9	10.00	11.7
CB effective density of states ($1/\text{cm}^3$)	2.5×10^{21}	1×10^{19}	2.5×10^{20}
VB effective density of states ($1/\text{cm}^3$)	2.5×10^{21}	1×10^{18}	2.5×10^{20}
Electron thermal velocity (cm/s)	1.0×10^{07}	1×10^{07}	1×10^{07}
Hole thermal velocity (cm/s)	1.0×10^{07}	1×10^{07}	1×10^{07}
Electron mobility (cm^2/Vs)	0.20	1.6	2.8
Hole mobility (cm^2/Vs)	0.20	1.6	2.8
Shallow uniform acceptor density, N_A ($1/\text{cm}^3$)	0.00	3×10^{17}	3×10^{18}
Shallow uniform donor density, N_D ($1/\text{cm}^3$)	2.930×10^{17}	3×10^{17}	0.00
Defect type	Neutral	Neutral	Neutral
Capture cross section electrons (cm^2)	1×10^{-15}	1×10^{-15}	1×10^{-15}
Capture cross section holes (cm^2)	1×10^{-15}	1×10^{-15}	1×10^{-15}
Energetic distribution	Single	Single	Single
Reference for defect energy level E_t	Above E_v	Above E_v	Above E_v
Energy level with respect to Reference (eV)	0.600	0.600	0.600
N_t total ($1/\text{cm}^3$) uniform	1×10^{14}	1×10^{14}	1×10^{14}

Table 3
Effect of different back contact metal.

Back contact metal	Al	Sn	Ag	Fe	Cu
Metal Work function (eV)	4.26	4.42	4.74	4.81	5.00

Table 4
The simulated results of PV parameters of $\text{CH}_3\text{NH}_3\text{SnI}_3$ based inverted PSC using SCAPS-1D.

Voc, V	Jsc, mA/cm ²	FF, %	PCE, %
0.9756	33.45	70.33	22.95

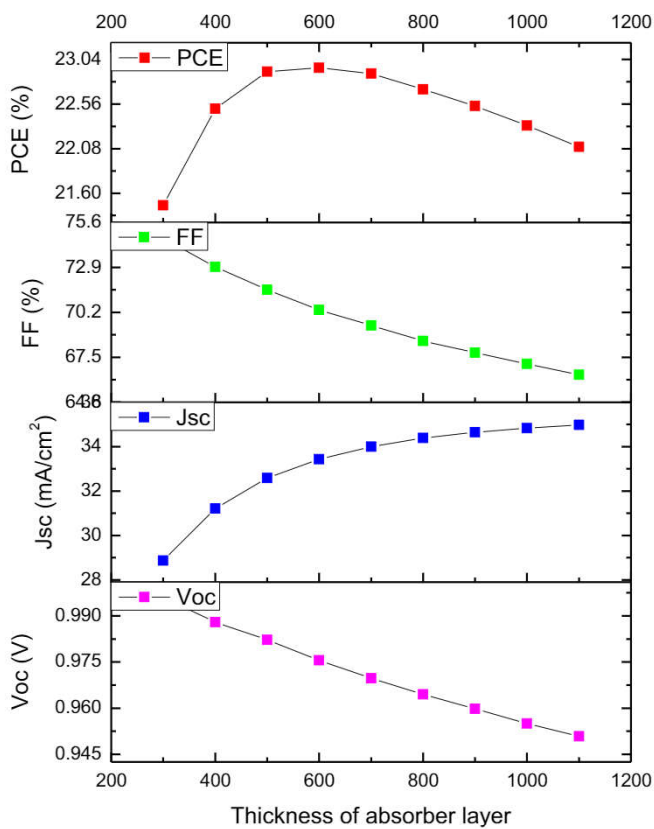


Fig. 3. Effect of perovskite layer thickness on PV parameters.

as the ETM layer. Fig. 3 represents the variation of photovoltaic parameters with the thickness of perovskite layer. It is found that as the thickness of perovskite layer is increased, the efficiency of the solar cell increases up to a certain value, which is considered as optimum thickness for the solar cell, and beyond that value efficiency decreases. As a thicker absorber layer absorb more photons, with increase in thickness there results increase in the short circuit current (Jsc). But in a thicker absorber layer as the charges have to travel longer distance for diffusion, the chance of recombination increases. So after a certain value of thickness, efficiency decreases. This result is in agreement with the experimental result by Correa-Baena et al. [15]. Accelerated recombination with increase in thickness causes declination of Voc. A 600 nm thick absorber layer is optimum to get high PCE for inverted PSC as seen in Fig. 3. ETM and HTM layers haven't any effect on photovoltaic (PV) parameters. Figs. 4 and 5 illustrates the simulated result of it.

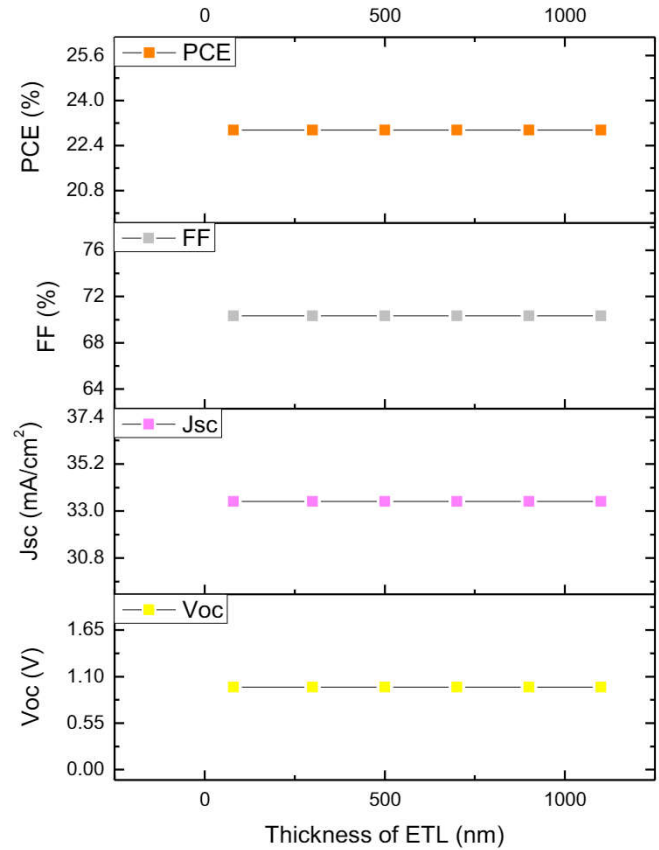


Fig. 4. Effect of ETL thickness on PV parameters.

3.2. Effect of different back contact material

Simulation have been done using aluminium (Al), tin (Sn), silver (Ag), iron (Fe) and copper (Cu) as back contact for inverted PSC. Fig. 6 illustrates the simulation result of efficiency for different back contact materials. The performance of the solar cell decreases with increasing work function of metal used. With increase in metal work function, the majority carrier barrier height increases, thus efficiency decreases. Table 3 shows effect of various metal contacts on efficiency of the cell. Al is the most suitable back contact in inverted PSC.

3.3. Effect of the defect state of the interface defect layers PCBM/ $\text{CH}_3\text{NH}_3\text{SnI}_3$ and $\text{CH}_3\text{NH}_3\text{SnI}_3/\text{NiO}$

Two defect layers have been considered for the simulations of the proposed inverted PSC structure. Numerical simulation study has been performed on the defect density at the interface of PCBM/ $\text{CH}_3\text{NH}_3\text{SnI}_3$ from $1 \times 10^{10} \text{ cm}^{-3}$ to $1 \times 10^{16} \text{ cm}^{-3}$ and that of $\text{CH}_3\text{NH}_3\text{SnI}_3/\text{NiO}$ from $1 \times 10^{10} \text{ cm}^{-3}$ to $8 \times 10^{10} \text{ cm}^{-3}$. Figs. 7 and 8 shows the effect of interface defect density on PV parameters. As increase in defect density causes increase in recombination rate, efficiency decreases considerably. From the simulated results the interface defect density of $1 \times 10^{10} \text{ cm}^{-3}$ is optimum for device simulation.

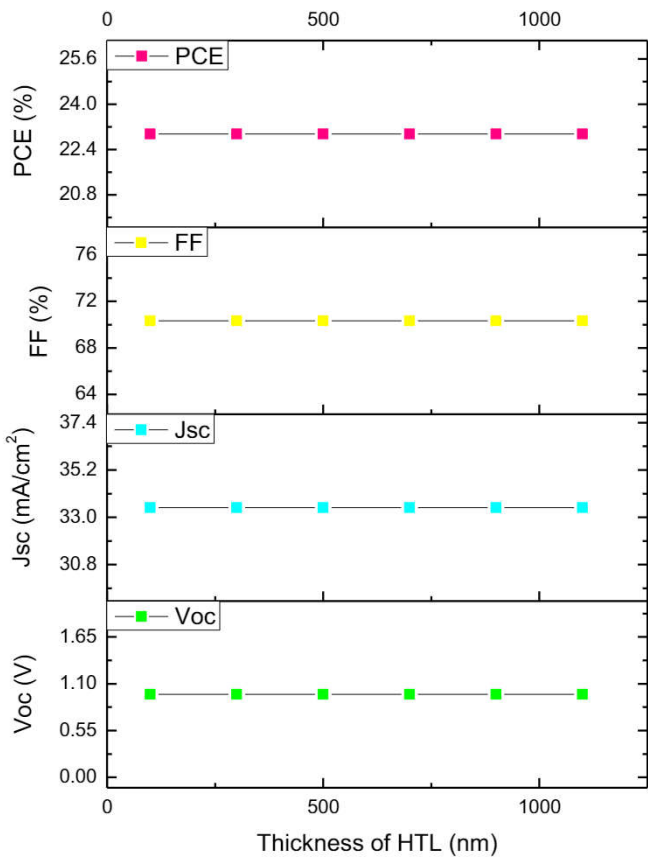


Fig. 5. Effect of HTL thickness on PV parameters.

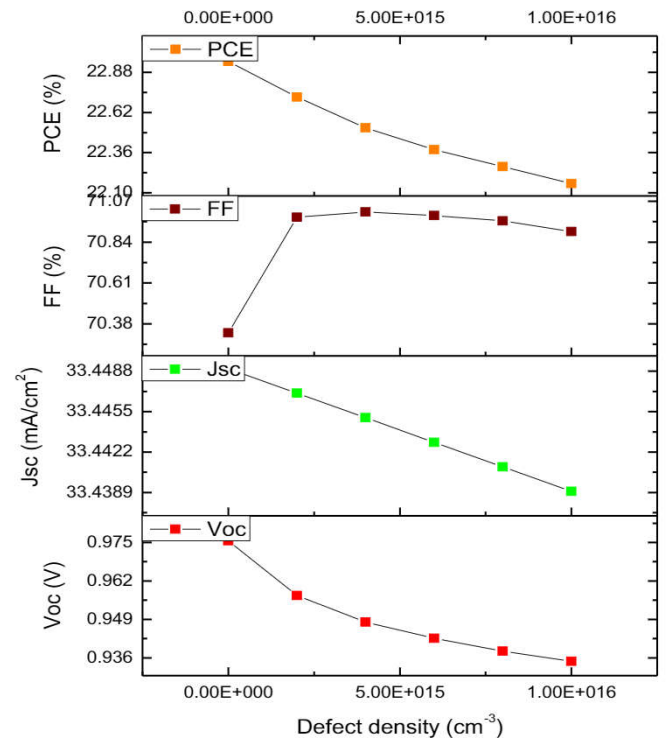


Fig. 7. Effect of the Defect State of the interface defect layer PCBM/CH₃NH₃SnI₃.

3.4. Effect of density of states (DOS) on the absorber layer

To discern the effect of DOS on the absorber layer the valance band effective density of states (N_v) has been varied from $1 \times 10^{18} \text{ cm}^{-3}$ to and $1 \times 10^{19} \text{ cm}^{-3}$ and conduction band effective

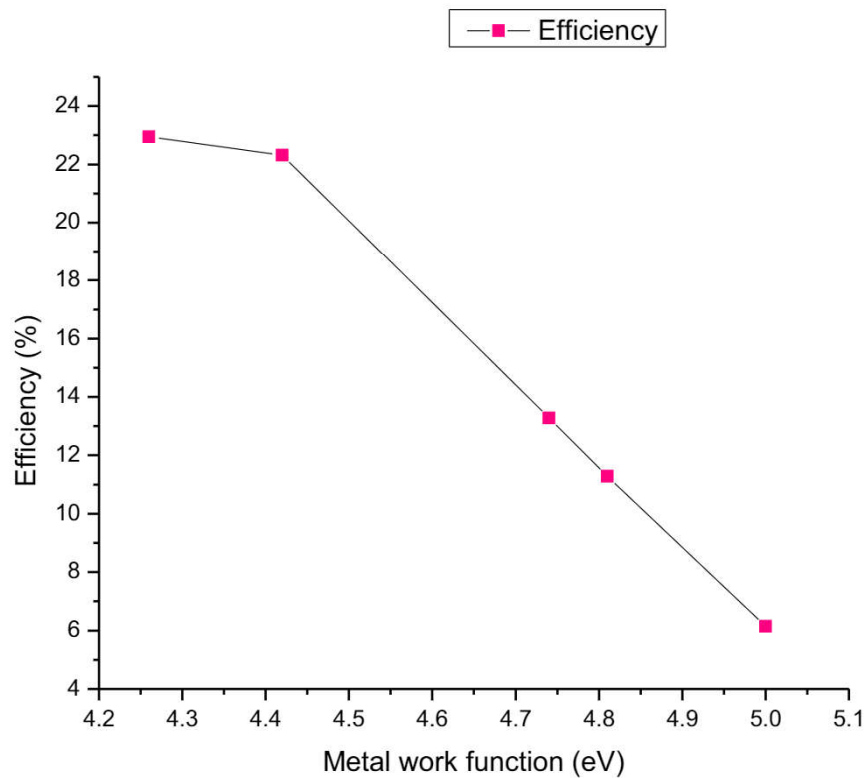


Fig. 6. Effect of different back metal contact on efficiency.

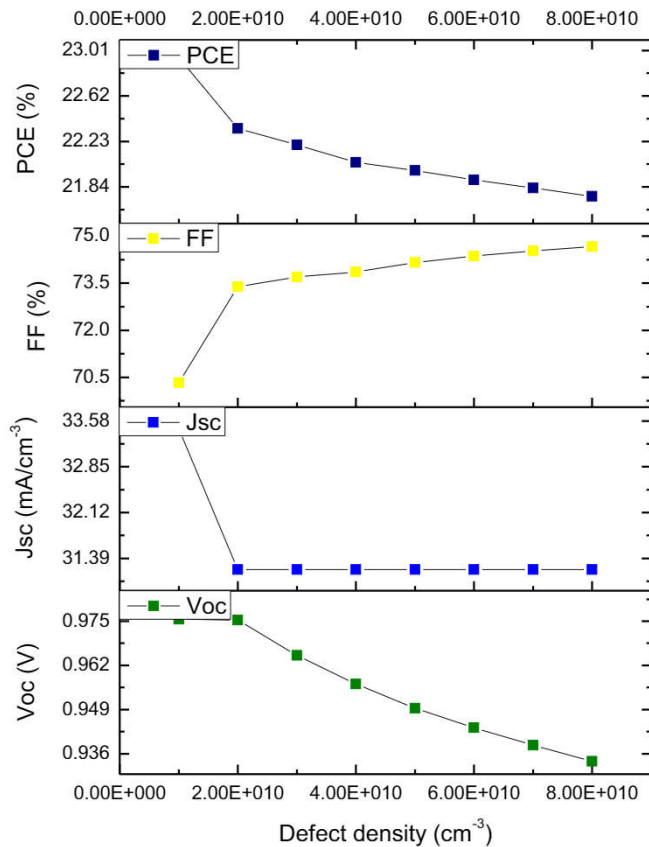


Fig. 8. Effect of the Defect State of the interface defect layer $\text{CH}_3\text{NH}_3\text{SnI}_3/\text{NiO}$.

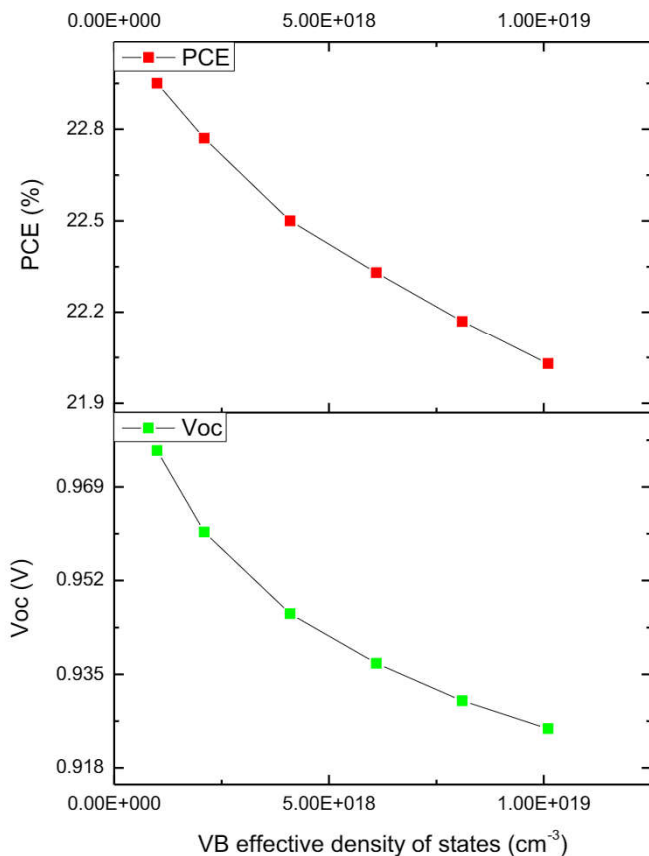


Fig. 9. Effect of valance band effective density of state on Voc and efficiency.

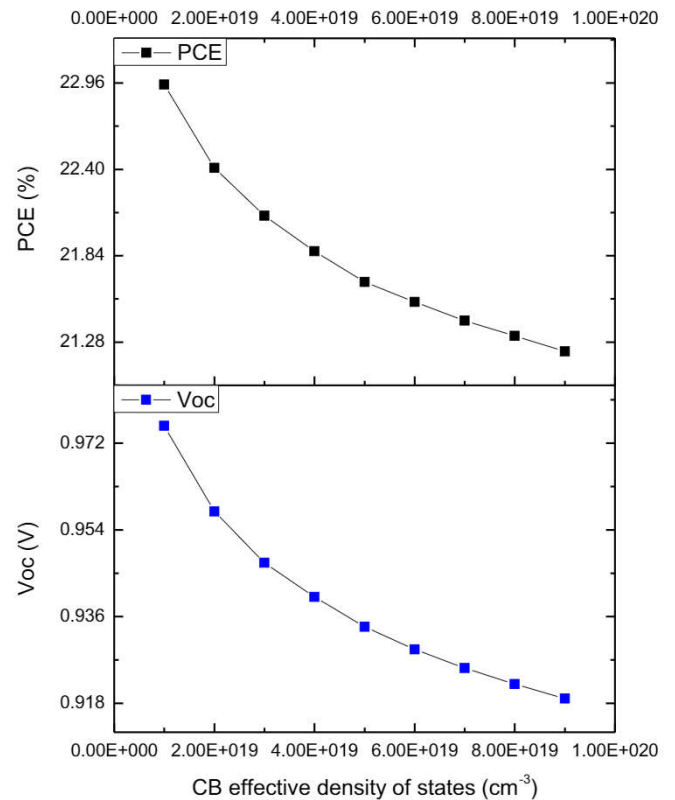


Fig. 10. Effect of conduction band effective density of state on Voc and efficiency.

density of states (N_c) from $1 \times 10^{19} \text{ cm}^{-3}$ to $9 \times 10^{19} \text{ cm}^{-3}$. As DOS increases chances of recombination, reverse saturation current and scattering increases. This will result in the decrease in efficiency of the solar cell. Figs. 9 and 10 show the variation of efficiency and Voc with N_v and N_c respectively.

4. Conclusion

The lead free $\text{CH}_3\text{NH}_3\text{SnI}_3$ based inverted PSC has been simulated using one-dimensional solar cell simulator SCAPS-1D, with PCBM as ETL and NiO as HTL. From the simulations, it has been deduced that the proposed cell have very good efficiency of 22.95%. The simulation results show that the optimized absorber layer thickness is 600 nm. A downfall of efficiency has been noticed with the increase of defect density of the interface layers (PCBM/ $\text{CH}_3\text{NH}_3\text{SnI}_3$) and ($\text{CH}_3\text{NH}_3\text{SnI}_3/\text{NiO}$). Different back contact metals were used to study simulation effect on the performance of the model. Cell performance improves greatly with the reduction of effective density of states of valance and conduction bands. From the result of the simulations, it can be summarized that ITO/NiO/ $\text{CH}_3\text{NH}_3\text{SnI}_3/\text{PCBM}/\text{Al}$ inverted PSC structure is a potential alternative for the third generation solar cell which can be reasonably efficient.

Declaration of Competing Interest

The authors declare that they have no known competing financial interests or personal relationships that could have appeared to influence the work reported in this paper.

Acknowledgements

The authors would like to thank Marc Burgelman, Department of Electronics and Systems, University of Gent, for the access of

SCAPS software. One of the authors Ms. Shamna M. S. would like to thank The Council of Scientific and Industrial Research (CSIR), India for the junior research fellowship.

References

- [1] P. Gao, M. Grätzel, M.K. Nazeeruddin, Organohalide lead perovskites for photovoltaic applications, *Energy Environ. Sci.* 7 (2014) 2448–2463, <https://doi.org/10.1039/c4ee00942h>.
- [2] NREL, Best Research-Cell Efficiencies, 2019. http://www.nrel.gov/ncpv/images/efficiency_chart.jpg.
- [3] P. Umari, E. Mosconi, F. De Angelis, Relativistic GW calculations on $\text{CH}_3\text{NH}_3\text{PbI}_3$ and $\text{CH}_3\text{NH}_3\text{SnI}_3$ perovskites for solar cell applications, *Sci. Rep.* 4 (2014) 4467–4473, <https://doi.org/10.1038/srep04467>.
- [4] H.-J. Du, W.-C. Wang, J.-Z. Zhu, Device simulation of lead-free $\text{CH}_3\text{NH}_3\text{SnI}_3$ perovskite solar cells with high efficiency, *Chin. Phys. B* 25 (2016), <https://doi.org/10.1088/1674-1056/25/10/108802> 108802.
- [5] B. Chen, M. Yang, S. Priya, K. Zhu, Origin of J-V hysteresis in perovskite solar cells, *J. Phys. Chem. Lett.* 7 (2016) 905–917, <https://doi.org/10.1021/acs.jpcllett.6b00215>.
- [6] Z. Xiao, Y. Yuan, Y. Shao, Q. Wang, Q. Dong, C. Bi, P. Sharma, A. Gruverman, J. Huang, Giant switchable photovoltaic effect in organometal trihalide perovskite devices, *Nat. Mater.* 14 (2014) 193–198, <https://doi.org/10.1038/NMAT4150>.
- [7] H. Zhang, C. Liang, Y. Zhao, M. Sun, H. Liu, J. Liang, D. Li, F. Zhang, Z. He, Dynamic interface charge governing the current–voltage hysteresis in perovskite solar cells, *Phys. Chem. Chem. Phys.* 17 (2015) 9613–9618, <https://doi.org/10.1039/c5cp00416k>.
- [8] S. Ye, H. Rao, Z. Zhao, L. Zhang, H. Bao, W. Sun, Y. Li, F. Gu, J. Wang, Z. Liu, Z. Bian, C. Huang, A breakthrough efficiency of 19.9% obtained in inverted perovskite solar cells by using an efficient trap state passivator $\text{Cu}(\text{thiourea})\text{I}$, *J. Am. Chem. Soc.* 139 (2017) 7504–7512, <https://doi.org/10.1021/jacs.7b01439>.
- [9] Y. Shao, Z. Xiao, C. Bi, Y. Yuan, J. Huang, Origin and elimination of photocurrent hysteresis by fullerene passivation in $\text{CH}_3\text{NH}_3\text{PbI}_3$ planar heterojunction solar cells, *Nat. Commun.* 5 (2014) 5784, <https://doi.org/10.1038/ncomms6784>.
- [10] J. Xu, A. Buin, A.H. Ip, W. Li, O. Voznyy, R. Comin, M. Yuan, S. Jeon, Z. Ning, J.J. McDowell, P. Kanjanaboos, J.P. Sun, X. Lan, L.N. Quan, D.H. Kim, I.G. Hill, P. Maksymovych, E.H. Sargent, Perovskite–fullerene hybrid materials suppress hysteresis in planar diodes, *Nat. Commun.* 6 (2015) 7081, <https://doi.org/10.1038/ncomms8081>.
- [11] W. Yan, S. Ye, Y. Li, W. Sun, H. Rao, Z. Liu, Z. Bian, C. Huang, Hole-transporting materials in inverted planar perovskite solar cells, *Adv. Energy Mater.* 6 (2016) 1600474, <https://doi.org/10.1002/aenm.201600474>.
- [12] M. Burgelman, K. Decock, A. Niemegeers, J. Verschraegen, S. Degrave, *SCAPS Manual*, 2018.
- [13] J. Gong, S. Krishnan, Simulation of inverted perovskite solar cells, in: *ASME 2018 12th International Conference on Energy Sustainability*, 2018, <https://doi.org/10.1115/ES2018-7227>.
- [14] H.K. Yoo, H. Lee, K. Lee, C. Kang, C.-S. Kee, I.-W. Hwang, J.W. Lee, Conditions for Optimal Efficiency of PCBM-Based Terahertz Modulators 7 (2017) 105008, <https://doi.org/10.1063/1.5001561>.
- [15] J.-P. Correa-Baena, M. Anaya, G. Lozano, et al., Unbroken perovskite: interplay of morphology, electro-optical properties, and ionic movement, *Adv. Mater.* 28 (2016) 5031–5037, <https://doi.org/10.1002/adma.201600624>.